JACS
JOURNAL OF THE AMERICAN CHEMICAL SOCIETY
pubs.acs.org/JACS
Article

Bimolecular Coupling in Olefin Metathesis: Correlating Structure and Decomposition for Leading and Emerging Ruthenium–Carbene Catalysts

Daniel L. Nascimento, Marco Foscato, Giovanni Occhipinti, Vidar R. Jensen,* and Deryn E. Fogg*

Cite This: J. Am. Chem. Soc. 2021, 143, 11072–11079
Read Online
ACCESS | Metrics & More | Article Recommendations | Supporting Information

ABSTRACT: Bimolecular catalyst decomposition is a fundamental, long-standing challenge in olefin metathesis. Emerging ruthenium–cyclic(alkyl)-(amino)carbene (CAAC) catalysts, which enable breakthrough advances in productivity and general robustness, are now known to be extraordinarily susceptible to this pathway. The details of the process, however, have hitherto been obscure. The present study provides the first detailed mechanistic insights into the steric and electronic factors that govern bimolecular decomposition. Described is a combined experimental and theoretical study that probes decomposition of the key active species, $RuCl_2(L)(py)(=CH_2)$ **1** (in which L is the N-heterocyclic carbene (NHC) H_2IMes, or a CAAC ligand: the latter vary in the NAr group (NMes, N-2,6-$Et_2C_6H_3$, or N-2-Me,6-$^iPrC_6H_3$) and the substituents on the quaternary site flanking the carbene carbon (i.e., CMe_2 or CMePh)). The transiently stabilized pyridine adducts **1** were isolated by cryogenic synthesis of the metallacyclobutanes, addition of pyridine, and precipitation. All are shown to decompose via second-order kinetics at −10 °C. The most vulnerable CAAC species, however, decompose more than 1000-fold faster than the H_2IMes analogue. Computational studies reveal that the key factor underlying accelerated decomposition of the CAAC derivatives is their stronger trans influence, which weakens the Ru–py bond and increases the transient concentration of the 14-electron methylidene species, $RuCl_2(L)(=CH_2)$ **2**. Fast catalyst initiation, a major design goal in olefin metathesis, thus has the negative consequence of accelerating decomposition. Inhibiting bimolecular decomposition offers major opportunities to transform catalyst productivity and utility, and to realize the outstanding promise of olefin metathesis.

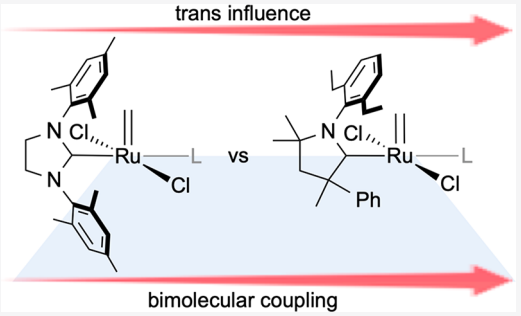

INTRODUCTION

Olefin metathesis offers exceptional versatility in the catalytic assembly of carbon–carbon bonds.[1,2] Recent advances hold great promise for overcoming productivity challenges in frontier applications, including pharmaceutical manufacturing,[3] materials science,[4,5] and chemical biology.[6] Notwithstanding the groundbreaking impact of the dominant Ru–H_2IMes catalysts, their facile decomposition is a fundamental limitation.[7] Of major importance, therefore, is the breakthrough performance of cyclic (alkyl)(amino) carbene derivatives (CAAC; Chart 1).[8] The CAAC catalysts show unprecedented productivity in the transformation of renewable fatty acids into α-olefins by cross-metathesis with ethylene ("ethenolysis"),[9−12] as first reported by Bertrand and Grubbs in 2015,[10] and in macrocyclization via ring-closing metathesis[11−13] (mRCM). The latter process is of highly topical interest for the production of antiviral drugs.[3]

Leading Ru–H_2IMes catalysts were long thought to initiate too slowly to decompose via bimolecular coupling of methylidene species **2** (Scheme 1a).[14,15] This is not the case: bimolecular decomposition is now known to compete with the general, well-established β-hydride elimination pathway[16,17] shown in Scheme 1b.[18] Indeed, we recently reported that the Ru-CAAC catalysts resist β-hydride elimination, but appear highly sensitive to bimolecular decomposition.[18a] This would account for the sometimes striking drop in metathesis productivity evident when catalyst loadings are increased.[19] In studies of transiently stabilized methylidene species, we demonstrated that bimolecular coupling is significantly faster for the CAAC catalyst **1-C1^{Ph}** than its H_2IMes analogue **1-H_2IMes**.[20] To date, the factors that govern this pathway remain poorly understood. Although bimolecular coupling is a general vector for decomposition of both early and late transition methylidene species,[14−16,18] many details remain obscure. Here we present an experimental and computational study that provides the first detailed insight into the process, and its sensitivity to the nature of the neutral carbene ligand.

Received: April 29, 2021
Published: July 16, 2021

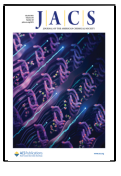

https://doi.org/10.1021/jacs.1c04424
J. Am. Chem. Soc. 2021, 143, 11072–11079

Chart 1. Catalysts and Carbene Ligands Discussed[a]

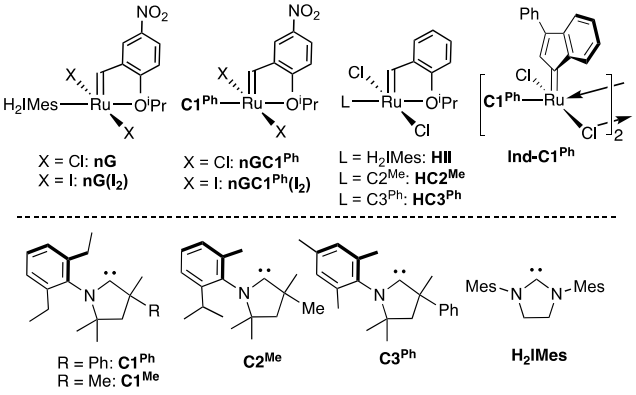

[a]The CAAC labeling system adopted (C#[R]) defines ligand families by common NAr moiety. The superscript R specifies the fourth substituent on the quaternary site flanking the carbene carbon.

Scheme 1. Intrinsic Decomposition Pathways: (a) Bimolecular Decomposition; (b) β-Hydride Elimination[a]

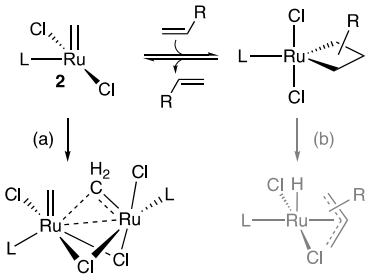

[a]Path (b) was found to be negligible for L = $\mathbf{C1^{Ph}}$ and $\mathbf{C2^{Me}}$: see text.

These findings are expected to aid both strategic planning and de novo catalyst design.[21,22]

The key experimental evidence for bimolecular coupling of $RuCl_2(L)(py)(=CH_2)$ (L = H_2IMes, $\mathbf{C1^{Ph}}$) in our prior work was the liberation of ethylene from the isolated pyridineadducts in ca. 80% yield.[18a,b] Essential for quantitation was rapid warming of the samples from −20 °C to rt, to minimize loss of ethylene to the headspace. In the present study, we sought to probe the relevant structure−decomposition relationships, by assessing the relative susceptibility to bimolecular coupling of the series of CAAC and H_2IMes complexes shown in Chart 1. We began with a kinetics study of the isothermal decomposition of these transiently stabilized complexes at −10 °C.

RESULTS AND DISCUSSION

The methylidene species were synthesized via the cryogenic protocol of Scheme 2,[18a,b] in which the Piers phosphonium alkylidenes were treated with ethylene to form the metallacyclobutane **MCB**,[17a,23] then with pyridine to collapse the ring and form the pyridine adducts **1**. The phosphonium ylide coproduct, $[H_2C{=}CHP^iPr_3]OTf$, was precipitated by cannula addition of cold (−110 °C) hexanes, and removed by filtration. Evaporation of the filtrate enabled isolation of the py adducts for all but $\mathbf{1\text{-}C2^{Me}}$. The latter was formed, as indicated by observation of the diagnostic ^1H NMR signal for the [Ru]$=CH_2$ protons at 18.22 ppm (Figure S18), but was too unstable to isolate.

Scheme 2. Synthesis of Transiently Stabilized Methylidene Complexes $RuX_2(L)(py)(=CH_2)$, 1[a]

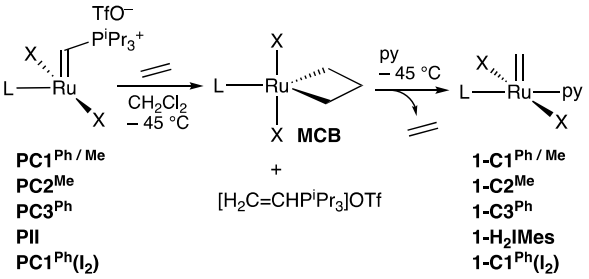

[a]L = $\mathbf{C1^{Ph}}$, $\mathbf{C1^{Me}}$, $\mathbf{C2^{Me}}$, $\mathbf{C3^{Ph}}$, H_2IMes. X = Cl in all cases except $RuI_2(\mathbf{C1^{Ph}})(py)(=CH_2)$.

With this set of five methylidene complexes in hand, we undertook NMR studies to establish their relative susceptibility to bimolecular decomposition. Accordingly, each was redissolved at −35 °C in a solution of $CDCl_3$ containing an integration standard of known concentration. The samples were warmed to −10 °C, and their rates of decomposition were monitored from the decline in the intensity of the methylidene signal relative to that for the internal standard. Second-order kinetics were observed (Figure 1), confirming that decomposition is dominated by bimolecular coupling. The second-order rate constants spanned 3 orders of magnitude, with coupling being slowest for $\mathbf{1\text{-}H_2IMes}$ and ≫1200 times faster for $\mathbf{1\text{-}C2^{Me}}$. The lower limit for the latter is set by the rate for $\mathbf{1\text{-}C1^{Me}}$, the fastest-decomposing species for which a rate could be measured.

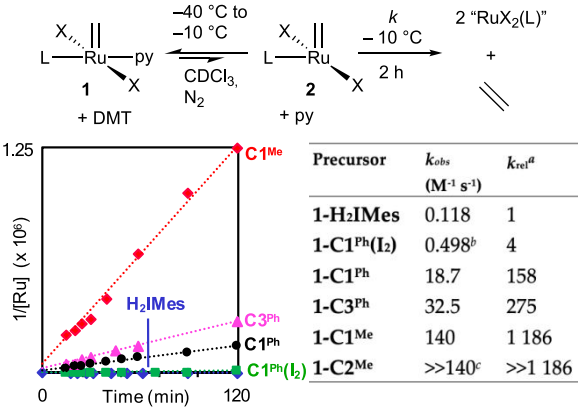

Precursor	k_{obs} (M^{-1} s^{-1})	k_{rel}[a]
$\mathbf{1\text{-}H_2IMes}$	0.118	1
$\mathbf{1\text{-}C1^{Ph}(I_2)}$	0.498[b]	4
$\mathbf{1\text{-}C1^{Ph}}$	18.7	158
$\mathbf{1\text{-}C3^{Ph}}$	32.5	275
$\mathbf{1\text{-}C1^{Me}}$	140	1 186
$\mathbf{1\text{-}C2^{Me}}$	>>140[c]	>>1 186

Figure 1. Second-order plot for bimolecular decomposition, and tabulated rate constants (k_{obs}). Average of two trials.[24] [a]k_{rel} = rate constants normalized to that for the slowest-decomposing system, $\mathbf{1\text{-}H_2IMes}$. DMT = dimethyl terephthalate (internal standard). [b]A similar rate (0.444 M^{-1} s^{-1}) was observed in C_7D_8. [c]A lower limit is given for $\mathbf{1\text{-}C2^{Me}}$, which decomposed too rapidly to isolate.

Figure 2 highlights the impact of individual structural features on rates of decomposition. We first consider the impact of the NAr *o*-aryl substituents, within CAAC ligands bearing a CMePh group adjacent to the carbene carbon (Figure 2a). The *N*-mesityl complex $\mathbf{1\text{-}C3^{Ph}}$ decomposes at twice the rate of its *N*-diethylphenyl (N-DEP) analogue $\mathbf{1\text{-}C1^{Ph}}$. That is, the rate of coupling is doubled by removing just one methylene unit from each *o*-substituent. (The mesityl *p*-methyl substituent in $\mathbf{C3^{Ph}}$ may also play a role, for example by increasing σ-donation slightly relative to $\mathbf{C1^{Ph}}$, but this effect is

https://doi.org/10.1021/jacs.1c04424
J. Am. Chem. Soc. 2021, 143, 11072−11079

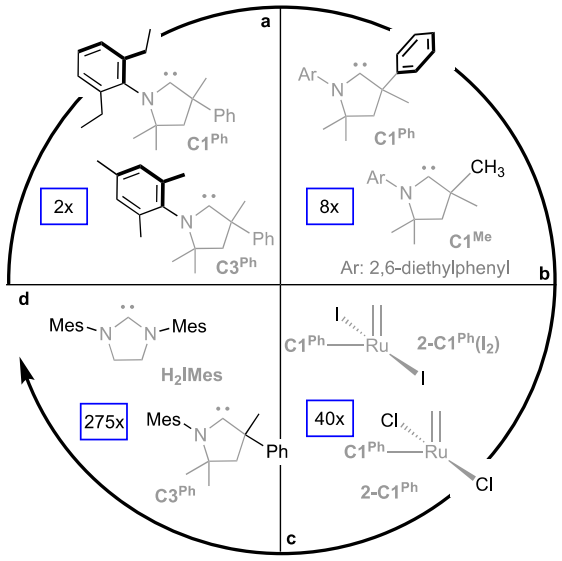

Figure 2. Relative rates (text in blue boxes) of bimolecular decomposition as a function of the structural changes shown in black: (a) NAr substituents. (b) Substitution at C_α (the quaternary center α to the carbene carbon). (c) The anionic ligand: chloride vs iodide. (d) NHC vs CAAC: H_2IMes vs its closest analogue, **C3^{Ph}**.

presumed to be minor.) Faster decomposition with diminishing NAr bulk would account for the lower productivity reported for multiple catalyst classes (including Hoveyda, Grela, and bis-CAAC platforms) when the **C1^{Ph}** ligand is replaced with **C3^{Ph}**.[10,12,13]

Truncation of the quaternary CMePh group to CMe_2 (**1-C1^{Ph}** vs **1-C1^{Me}**; see Figure 2b) triggers both steric and electronic impacts. The N-DEP group is then too small to retard coupling, and **1-C1^{Me}** decomposes nearly 10× faster than **1-C1^{Ph}**. Consistent with this trend are the lower turnover numbers reported for **C1^{Me}** catalysts relative to their **C1^{Ph}** analogues in multiple contexts, ranging from ethenolysis to acrylonitrile metathesis.[12,13,25]

Of note in this context is the much faster decomposition seen for **1-C2^{Me}**, despite the presence of one relatively bulky *o*-^{i}Pr substituent. Computational examination (see below) revealed that the latter in fact promotes pyridine loss to form the four-coordinate species **2-C2^{Me}**, while being insufficient to impede coupling. The extreme sensitivity of the **C2^{Me}** catalysts to bimolecular decomposition is implied by multiple experimental studies, as we have noted elsewhere.[18,26] Perhaps most striking is the negative impact of increased catalyst loadings on TONs for **HC2^{Me}** even at <5 ppm catalyst.[10,27] Indeed, bimolecular coupling of **HC2^{Me}** appears to be so rapid at 70 °C that nucleophilic abstraction of the methylidene ligand is unable to compete, even when aggressive[28] nucleophiles such as unencumbered primary amines are employed.[26]

An inherent trade-off is thus apparent between the steric protection required to retard bimolecular decomposition and the steric accessibility required for fast initiation and turnover. As illustrated in Figure 2c, replacing the chloride ligands in the **C1^{Ph}** derivative by iodide slows the rate of decomposition 40-fold. Iodide catalysts, long overlooked because of their lower reactivity,[29] have recently been shown to offer productivity superior to their faster-initiating analogues in demanding contexts that require long catalyst lifetimes.[19b,30−33] Retarded bimolecular decomposition is clearly an important component of this robustness, although it should be noted that coupling remains operative for **nG(I$_2$)** even at micromolar catalyst concentrations.[19b] Slowly initiating CAAC-iodide metathesis catalysts may thus be of keen interest for metathesis of accessible olefinic bonds, although few such complexes have yet been developed.[8a,33]

We come last to a more difficult comparison (Figure 2d), between **1-H$_2$IMes** and its closest CAAC analogue, **1-C3^{Ph}**. The superficially minor replacement of one H_2IMes N-mesityl group by a CMePh unit dramatically increases the rate constant for decomposition, by 275×. Multiple parameters are affected by the transformation of an NHC to even a closely corresponding CAAC ligand, a point that has seen much recent discussion.[8a,34−37] To probe the specific impact on bimolecular decomposition, we turned to computational analysis.

A density functional theory (DFT) analysis of the bimolecular coupling of **1-H$_2$IMes** reveals a complex overall mechanism. Key intermediates and transition states are shown in Scheme 3, with details in the SI. Full exploration for the

Scheme 3. Key Steps in the Bimolecular Decomposition of 1 Identified by DFT Calculations

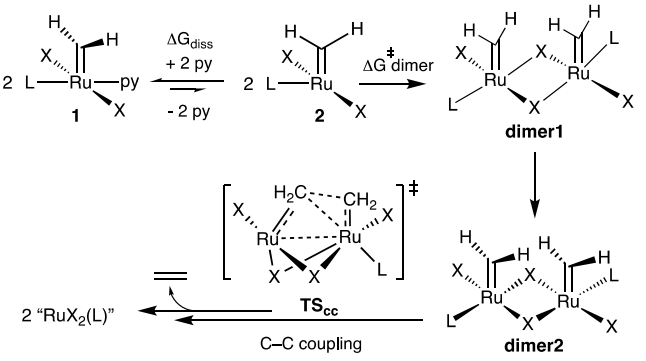

CAAC complexes is hampered by the multitude of isomers arising from the unsymmetrical nature of the carbene, and the chiral centers present in **C1^{Ph}** and **C3^{Ph}**. We therefore limited study of the CAAC systems to the Ru species of Scheme 3, with diruthenium structures being further limited to the diastereomeric dimers and transition states of **1-C3^{Ph}**. Even with these restrictions, the study included 16 unique structures for the C−C bond-forming transition state (**TS$_{CC}$**) alone. The free energies in Table 1 were calculated using experimental catalyst concentrations: free energies calculated at 1 mM for all catalysts are provided in the Supporting Information (SI).

The calculations suggest that bimolecular decomposition is controlled by a few key steps (Scheme 3). Even the initial ligand dissociation is important, as indicated by the inverse correlation between the rate constants for decomposition in Figure 1 and the free-energy changes for pyridine dissociation in Table 1. Thus, the highest penalty for loss of pyridine (ΔG_{diss} = 7.6 kcal/mol) is found for **1-H$_2$IMes**, which is experimentally most resistant to bimolecular decomposition. Pyridine binding is ca. 3−10 kcal/mol weaker in the CAAC complexes, and the Ru−N bond distances are 3−6 pm longer (see Table 1 and DFT-optimized structures in Figure 3). The impact of this difference will be doubled in the relative decomposition rates, as two pyridine ligands must be lost for a single dimer to form.

Weakening of the Ru−py bonds in the CAAC complexes is due chiefly to the enhanced σ-donor and π-acceptor character

https://doi.org/10.1021/jacs.1c04424
J. Am. Chem. Soc. 2021, 143, 11072−11079

Table 1. Calculated Free Energies and Buried Volumes[a]

Starting Complex	Pyridine Loss (ΔG_{diss})	Dimerization ($\Delta G^{\ddagger}_{dimer}$)	Buried Volume ($\%V_{bur}$)[b]
1-H$_2$IMes	7.6	19.5	81.9
1-C1^{Ph}(I$_2$)	4.4	13.2	88.6
1-C1^{Ph}	3.9	12.3	83.7
1-C3^{Ph}	3.8	12.1	82.6
1-C1^{Me}	0.4	5.1	83.7
1-C2^{Me}	−2.0	0.4	82.8

[a]Free energies in kcal/mol vs G(**1**), calculated for the most stable rotamers of **1** and **2** at experimental catalyst concentrations (**1-H$_2$IMes**: 1.4 mM, **1-C1^{Ph}(I$_2$)**: 0.59 mM, **1-C1^{Ph}**: 0.061 mM, **1-C3^{Ph}**: 0.027 mM, **1-C1^{Me}**: 0.01 mM). $\Delta G_{diss} = G(\mathbf{2}) + G(py) - G(\mathbf{1})$; $\Delta G^{\ddagger}_{dimer} = 2 \times \Delta G_{diss} + \Delta G^{\ddagger}_{diff}$ where $\Delta G^{\ddagger}_{diff}$ is the estimated lower limit for the free-energy barrier (4.4 kcal/mol). See SI for details. [b]$\%V_{bur}$ = fraction of the first coordination sphere (radius 3.5 Å) that is occupied in **2**.[38]

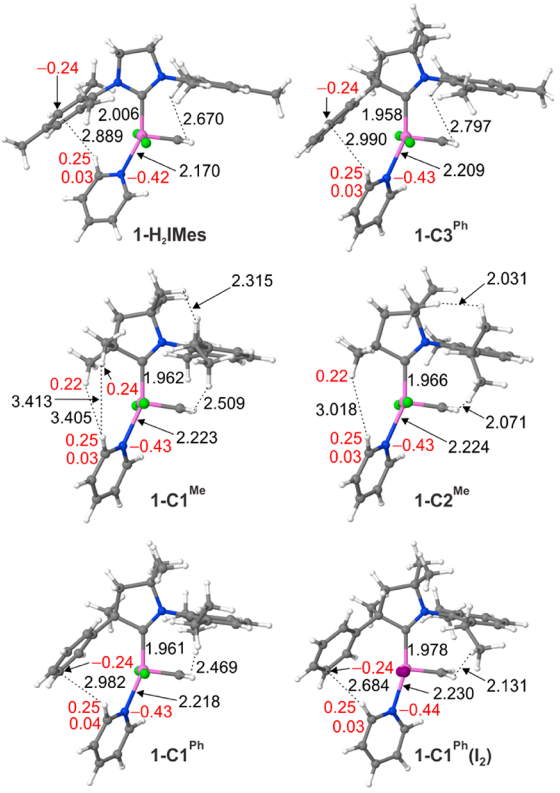

Figure 3. Selected atomic distances (Å) for py adducts **1** (DFT-optimized geometries). Ru: pink; Cl: green; I: violet; C: gray; N: blue; H: white). Natural charges (e) of selected atoms appear in red text.

of this carbene class,[8] which increases the trans influence of the CAAC ligands relative to NHCs. In **1-C1^{Ph}(I$_2$)**, the most stable of the CAAC species studied, the trans influence of **C1^{Ph}** is attenuated by the Ru−C$_{carbene}$ bond elongation induced by the bulky iodide ligands. The significant steric impact of the latter is evident from the much higher buried volume calculated for this complex (Table 1). The Ru−py bond in the iodide complex is hence 0.5 kcal/mol stronger than that in chloride analogue **1-C1^{Ph}**, contributing to the reduced susceptibility to bimolecular decomposition.

A significantly weaker Ru−py bond is seen in **1-C1^{Me}** and (in particular) **1-C2^{Me}**. Given the broad similarity in calculated buried volumes ($\%V_{bur}$; Table 1) for the various CAAC ligands,[39] this instability is unlikely to be steric in origin. Rather, we suggest that the key feature that distinguishes **C1^{Me}** and **C2^{Me}** is the absence of an aromatic quaternary substituent that can participate in polar CH−π interactions[40,41] with the pyridine ligand in **1**. In the most stable conformers of **1-C2^{Me}** and **1-C1^{Me}**, the N-aryl group is syn to the methylidene, precluding such interaction. In the **C1^{Ph}** and **H$_2$IMes** complexes, in comparison, an electron-rich aromatic ring is positioned to engage in hydrogen bonding and donor−acceptor bonding with the electron-deficient o-H and o-C pyridine atoms (natural charges = 0.25 e (H), 0.03−0.04 e (C); Figure 3).[42]

Importantly, these stabilizing interactions are not restricted to the pyridine ligand: they are likewise expected for bound olefin, owing to Ru-induced polarization of the sp^2 C−H bonds. The consequent reduction in the concentration of the 14-electron species would limit bimolecular decomposition.[43] For the CAAC catalysts to achieve these effects, however, a quaternary aromatic group is essential. In **1-C1^{Me}** and **1-C2^{Me}**, the hydrogen atoms of the quaternary methyl groups bear a positive charge, as do the pyridine o-H and o-C atoms: this and the minimum Me−pyridine interatomic distances (>3 Å; Figure 3) reflect the absence of attractive interactions.

An additional factor affecting **1-C2^{Me}**, beyond the absence of stabilizing polar CH−π interactions, is steric repulsion associated with the NAr o-isopropyl substituent. The latter is within ca. 2 Å of both the methylidene ligand and the methyl groups on the carbene backbone. Steric repulsion is relieved by pyridine dissociation and 90° rotation of the methylidene group to form **2**. The observed instability of **1-C2^{Me}** is thus due to a combination of steric and electronic factors.

The second-order kinetics evident in Figure 1 indicate that pyridine dissociation is not rate-limiting. Detailed calculations on **1-H$_2$IMes** and **1-C3^{Ph}** instead suggest that the rate-determining step is coupling of two molecules of 14-electron **2** to form **dimer1** (Scheme 3), in which a chloride from each Ru atom serves as a dative ligand to the other Ru atom. Within this dimer, the geometry of the individual Ru centers in **2** is largely conserved, including the essentially orthogonal disposition of the methylidene ligand relative to the RuCl$_2$ plane (Figures S20, S25). The minimal geometrical adaption needed for **2-H$_2$IMes** and **2-C3^{Ph}** suggests little to no enthalpic cost to formation of **dimer1** from **2**. A lower bound for the barrier to dimerization can be obtained by assuming that the rate is diffusion-controlled. Rate constants for diffusion in common organic solvents are on the order of 4×10^9 s^{-1},[44] from which a barrier ($\Delta G^{\ddagger}_{diff}$) of 4.4 kcal/mol can be extracted using the Eyring equation. Summing this value and the free energies of two 14-electron complexes **2** gives an estimated overall barrier to dimerization $\Delta G^{\ddagger}_{dimer}$ of ca. 19.5 kcal/mol for **1-H$_2$IMes** and 12.1 kcal/mol for **1-C3^{Ph}**, relative to **1**.

In contrast, the ensuing rearrangement from **dimer1** to the more stable, tightly bonded **dimer2** is essentially barrierless. In **dimer2**, the methylidene groups return to a conformation aligned with the RuCl$_2$ plane. All subsequent steps are facile compared to the initial dimerization. That is, the barrier to C−C bond formation via **TS$_{CC}$** is lower than that to formation of **dimer1** (Table S1), as is the subsequent formation of an ethylene-bridged Ru dimer, rearrangement to a η^2-ethylene complex, and release of ethylene and Ru decomposition products (Figures S21, S22). The calculations for **1-H$_2$IMes** and **1-C3^{Ph}** thus strongly suggest that the most energy-demanding step in bimolecular decomposition of the 14-

https://doi.org/10.1021/jacs.1c04424
J. Am. Chem. Soc. 2021, 143, 11072−11079

electron complexes **2** is the formation of **dimer1**, rather than the ensuing coupling of methylidene units. Errors on the order of 2−5 kcal/mol for the calculated barriers $\Delta G^{\ddagger}_{dimer}$ are expected, given the general accuracy of DFT-calculated relative free energies (see the SI) and the exclusion of enthalpic contributions to dimerization of **2** discussed above. These translate to orders-of-magnitude variation in the rate constants, owing to the exponential (Eyring) relationship between barriers and rate constants. The agreement between the calculated dimerization barriers and the experimental rate constants should thus be expected to be qualitative only. Nevertheless, the computational prediction of the kinetic bottleneck is supported by the qualitative, rank-order agreement between the calculated barriers and the experimental rate constants, as well as the second-order kinetics (Figure S1), which support dimerization as the rate-determining step in the overall reaction.

CONCLUSIONS

Bimolecular catalyst decomposition has long been recognized as a fundamental challenge in olefin metathesis. Leading ruthenium−carbene catalysts, initially thought to be immune, are now known to be extraordinarily susceptible, even at ppm catalyst loadings. The foregoing provides the first detailed mechanistic insights into the process, and the steric and electronic factors that govern decomposition. An experimental "catalyst susceptibility ranking" was established for the most productive CAAC and NHC catalysts, and qualitatively reproduced via DFT analysis, which revealed that dimerization of the 14-electron complex **2** is rate-determining. A major component of this barrier is ligand dissociation to generate **2**, dimerization of which is retarded surprisingly little even by relatively bulky carbene ligands. Fast catalyst initiation, aimed at rapid generation of metathesis-active **2**, is thus inextricably connected to accelerated bimolecular decomposition for state-of-the-art NHC and (particularly) CAAC catalysts. The striking susceptibility of the latter to bimolecular decomposition is shown to originate in the high trans influence of the CAAC ligand, which promotes formation of four-coordinate **2**. Very low catalyst concentrations are then necessary to restrict bimolecular decomposition. Inhibition of this major decomposition pathway offers major opportunities to transform catalyst productivity and scope, and to realize the outstanding promise of olefin metathesis.

ASSOCIATED CONTENT

Supporting Information

The Supporting Information is available free of charge at https://pubs.acs.org/doi/10.1021/jacs.1c04424.

Experimental details, NMR spectra, computational details and supplementary computational results and data (PDF)

AUTHOR INFORMATION

Corresponding Authors

Deryn E. Fogg − *Center for Catalysis Research & Innovation, and Department of Chemistry and Biomolecular Sciences, University of Ottawa, Ottawa, Canada K1N 6N5; Department of Chemistry, University of Bergen, N-5007 Bergen, Norway;* orcid.org/0000-0002-4528-1139; Email: dfogg@uottawa.ca, deryn.fogg@uib.no

Vidar R. Jensen − *Department of Chemistry, University of Bergen, N-5007 Bergen, Norway;* orcid.org/0000-0003-2444-3220; Email: Vidar.Jensen@uib.no

Authors

Daniel L. Nascimento − *Center for Catalysis Research & Innovation, and Department of Chemistry and Biomolecular Sciences, University of Ottawa, Ottawa, Canada K1N 6N5;* orcid.org/0000-0002-9363-2175

Marco Foscato − *Department of Chemistry, University of Bergen, N-5007 Bergen, Norway;* orcid.org/0000-0001-7762-6931

Giovanni Occhipinti − *Department of Chemistry, University of Bergen, N-5007 Bergen, Norway;* orcid.org/0000-0002-7279-6322

Complete contact information is available at: https://pubs.acs.org/10.1021/jacs.1c04424

Notes

The authors declare no competing financial interest.

The computational data set is available from the ioChem-BD repository[45] via 10.19061/iochem-bd-6-79.

ACKNOWLEDGMENTS

Dedicated to Christian Bruneau, in honour of his outstanding contributions to catalysis and sustainable chemistry. This work was funded by the Natural Sciences and Engineering Research Council of Canada (NSERC) and by the Research Council of Norway (RCN, via Projects 262370, 288135, 226244, NN2506K, and NS2506K). The Government of Ontario is thanked for an International Ontario Graduate Scholarship to D.L.N.

REFERENCES

(1) Grela, K. *Olefin Metathesis-Theory and Practice*; Wiley: Hoboken, NJ, 2014.

(2) Grubbs, R. H.; Wenzel, A. G. *Handbook of Metathesis*, 2nd ed.; Wiley-VCH: Weinheim, 2015.

(3) (a) Higman, C. S.; Lummiss, J. A. M.; Fogg, D. E. Olefin Metathesis at the Dawn of Uptake in Pharmaceutical and Specialty Chemicals Manufacturing. *Angew. Chem., Int. Ed.* **2016**, *55*, 3552−3565. (b) Yu, M.; Lou, S.; Gonzalez-Bobes, F. Ring-Closing Metathesis in Pharmaceutical Development: Fundamentals, Applications, and Future Directions. *Org. Process Res. Dev.* **2018**, *22*, 918−946. (c) Farina, V.; Horváth, A. Ring-Closing Metathesis in the Large-Scale Synthesis of Pharmaceuticals. In *Handbook of Metathesis*; Grubbs, R. H., Wenzel, A. G., Eds.; Wiley-VCH: Weinheim, 2015; Vol. 2, pp 633−658. (d) Fandrick, K. R.; Savoie, J.; Jinhua, N. Y.; Song, J. J.; Senanayake, C. H. Challenges and Opportunities for Scaling the Ring-Closing Metathesis Reaction in the Pharmaceutical Industry. In *Olefin Metathesis − Theory and Practice*; Grela, K., Ed.; Wiley: Hoboken, NJ, 2014; pp 349−366. For recent examples of oncology or antiviral drug candidates, see: (e) St-Pierre, G.; Cherney, A. H.; Chen, W.; Dong, X.; Dornan, P. K.; Griffin, D. J.; Houk, K. N.; Lin, J. B.; Osgood, S.; Elipe, M. V. S.; Timmons, H. C.; Xie, Y.; Tedrow, J. S.; Thiel, O. R.; Smith, A. G. Accelerated Development of a Scalable Ring-Closing Metathesis to Manufacture AMG 176 Using a Combined High-Throughput Experimentation and Computational Modeling Approach. *Org. Process Res. Dev.* **2021**, *25*, 442−451. (f) Cink, R. D.; Lukin, K. A.; Bishop, R. D.; Zhao, G.; Pelc, M. J.; Towne, T. B.; Gates, B. D.; Ravn, M. M.; Hill, D. R.; Ding, C.; Cullen, S. C.; Mei, J. Z.; Leanna, M. R.; Henle, J.; Napolitano, J. G.; Nere, N. K.; Chen, S.; Sheikh, A.; Kallemeyn, J. M. Development of the Enabling Route for Glecaprevir via Ring-Closing Metathesis. *Org. Process Res. Dev.* **2020**, *24*, 183−200.

(4) For selected recent advances in materials science applications, see: (a) Rizzo, A.; Peterson, G. I.; Bhaumik, A.; Kang, C.; Choi, T.-L. Sugar-Based Polymers from d-Xylose: Living Cascade Polymerization, Tunable Degradation, and Small Molecule Release. *Angew. Chem., Int. Ed.* **2021**, *60*, 849−855. (b) Foster, J. C.; Grocott, M. C.; Arkinstall, L. A.; Varlas, S.; Redding, M. J.; Grayson, S. M.; O'Reilly, R. K. It is Better with Salt: Aqueous Ring-Opening Metathesis Polymerization at Neutral pH. *J. Am. Chem. Soc.* **2020**, *142*, 13878−13885. (c) Debsharma, T.; Schmidt, B.; Laschewsky, A.; Schlaad, H. Ring-Opening Metathesis Polymerization of Unsaturated Carbohydrate Derivatives: Levoglucosenyl Alkyl Ethers. *Macromolecules* **2021**, *54*, 2720−2728. (d) Church, D. C.; Takiguchi, L.; Pokorski, J. K. Optimization of Ring-Opening Metathesis Polymerization (ROMP) under Physiologically Relevant Conditions. *Polym. Chem.* **2020**, *11*, 4492−4499. (e) Feist, J. D.; Xia, Y. Enol Ethers Are Effective Monomers for Ring-Opening Metathesis Polymerization: Synthesis of Degradable and Depolymerizable Poly(2,3-dihydrofuran). *J. Am. Chem. Soc.* **2020**, *142*, 1186−1189. (f) Varlas, S.; Foster, J. C.; O'Reilly, R. K. Ring-Opening Metathesis Polymerization-Induced Self-Assembly (ROMPISA). *Chem. Commun.* **2019**, *55*, 9066−9071. (g) Varlas, S.; Keogh, R.; Xie, Y.; Horswell, S. L.; Foster, J. C.; O'Reilly, R. K. Polymerization-Induced Polymersome Fusion. *J. Am. Chem. Soc.* **2019**, *141*, 20234−20248. (h) Debsharma, T.; Behrendt, F. N.; Laschewsky, A.; Schlaad, H. Ring-Opening Metathesis Polymerization of Biomass-Derived Levoglucosenol. *Angew. Chem., Int. Ed.* **2019**, *58*, 6718−6721. (i) Jung, K.; Ahmed, T. S.; Lee, J.; Sung, J. C.; Keum, H.; Grubbs, R. H.; Choi, T. L. Living beta-selective cyclopolymerization using Ru dithiolate catalysts. *Chem. Sci.* **2019**, *10*, 8955−8963. (j) Theunissen, C.; Ashley, M. A.; Rovis, T. Visible-Light-Controlled Ruthenium-Catalyzed Olefin Metathesis. *J. Am. Chem. Soc.* **2019**, *141*, 6791−6796. (k) Song, K.; Kim, K.; Hong, D.; Kim, J.; Heo, C. E.; Kim, H. I.; Hong, S. H. Highly Active Ruthenium Metathesis Catalysts Enabling Ring-Opening Metathesis Polymerization of Cyclopentadiene at Low Temperatures. *Nat. Commun.* **2019**, *10*, 3860. (l) Kang, E.-H.; Yu, S. Y.; Lee, I. S.; Park, S. E.; Choi, T.-L. Strategies to Enhance Cyclopolymerization using Third-Generation Grubbs Catalyst. *J. Am. Chem. Soc.* **2014**, *136*, 10508−10514. For applications in tissue engineering, see: (m) Merrett, K.; Liu, W.; Mitra, D.; Camm, K. D.; McLaughlin, C. R.; Liu, Y.; Watsky, M. A.; Li, F.; Griffith, M.; Fogg, D. E. Synthetic neoglycopolymer-recombinant human collagen hybrids as biomimetic crosslinking agents in corneal tissue engineering. *Biomaterials* **2009**, *30*, 5403−5408.

(5) For recent reviews, see: (a) Edwards, J. P.; Wolf, W. J.; Grubbs, R. H. The Synthesis of Cyclic Polymers by Olefin Metathesis: Achievements and Challenges. *J. Polym. Sci., Part A: Polym. Chem.* **2019**, *57*, 228−242. (b) Knall, A.-C.; Slugovc, C. Olefin Metathesis Polymerization. In *Olefin Metathesis-Theory and Practice*; Grela, K., Ed.; Wiley: Hoboken, NJ, 2014; pp 269−284. (c) Dong, Y.; Matson, J. B.; Edgar, K. J. Olefin Cross-Metathesis in Polymer and Polysaccharide Chemistry. *Biomacromolecules* **2017**, *18*, 1661−1676.

(6) For recent reviews of olefin metathesis in chemical biology, see: (a) Isenegger, P. G.; Davis, B. G. Concepts of Catalysis in Site-Selective Protein Modifications. *J. Am. Chem. Soc.* **2019**, *141*, 8005−8013. (b) Vinogradova, E. V. Organometallic Chemical Biology: An Organometallic Approach to Bioconjugation. *Pure Appl. Chem.* **2017**, *89*, 1619−1640. (c) Messina, M. S.; Maynard, H. D. Modification of Proteins using Olefin Metathesis. *Mater. Chem. Front.* **2020**, *4*, 1040−1051.

(7) Problems arising from decomposition of the readily handled Ru catalysts are extensively documented in process chemistry in pharma (particularly for mRCM: ref 3), and in molecular biology, where bioconjugation is described as a race between metathesis and decomposition (ref 6a), requiring use of the Ru complex in significant stoichiometric excess. Perhaps more surprisingly, recent reports in materials applications likewise flag challenges arising from decomposition, notwithstanding the greater steric protection of the active species. See, for example, refs 4a−k.

(8) For recent overviews of advances with Ru-CAAC catalysts in olefin metathesis, see: (a) Morvan, J.; Mauduit, M.; Bertrand, G.; Jazzar, R. Cyclic (Alkyl)(amino)carbenes (CAACs) in Ruthenium Olefin Metathesis. *ACS Catal.* **2021**, *11*, 1714−1748. (b) Melaimi, M.; Jazzar, R.; Soleilhavoup, M.; Bertrand, G. Cyclic (Alkyl)(amino)-carbenes (CAACs): Recent Developments. *Angew. Chem., Int. Ed.* **2017**, *56*, 10046−10068.

(9) Recent reviews of ethenolysis: (a) Bidange, J.; Fischmeister, C.; Bruneau, C. Ethenolysis: A Green Catalytic Tool to Cleave Carbon−Carbon Double Bonds. *Chem. - Eur. J.* **2016**, *22*, 12226−12244. (b) Spekreijse, J.; Sanders, J. P. M.; Bitter, J. H.; Scott, E. L. The Future of Ethenolysis in Biobased Chemistry. *ChemSusChem* **2017**, *10*, 470−482. (c) Biermann, U.; Bornscheuer, U. T.; Feussner, I.; Meier, M. A. R.; Metzger, J. O., Fatty Acids and their Derivatives as Renewable Platform Molecules for the Chemical Industry. *Angew. Chem., Int. Ed.* **2021**, Early View article, DOI: 10.1002/anie.202100778.

(10) Marx, V. M.; Sullivan, A. H.; Melaimi, M.; Virgil, S. C.; Keitz, B. K.; Weinberger, D. S.; Bertrand, G.; Grubbs, R. H. Cyclic Alkyl Amino Carbene (CAAC) Ruthenium Complexes as Remarkably Active Catalysts for Ethenolysis. *Angew. Chem., Int. Ed.* **2015**, *54*, 1919−1923.

(11) Nascimento, D. L.; Gawin, A.; Gawin, R.; Guńka, P. A.; Zachara, J.; Skowerski, K.; Fogg, D. E. Integrating Activity with Accessibility in Olefin Metathesis: An Unprecedentedly Reactive Ruthenium-Indenylidene Catalyst Bearing a Cyclic Alkyl Amino Carbene. *J. Am. Chem. Soc.* **2019**, *141*, 10626−10631.

(12) Gawin, R.; Kozakiewicz, A.; Guńka, P. A.; Dąbrowski, P.; Skowerski, K. Bis(Cyclic Alkyl Amino Carbene) Ruthenium Complexes: A Versatile, Highly Efficient Tool for Olefin Metathesis. *Angew. Chem., Int. Ed.* **2017**, *56*, 981−986.

(13) Gawin, R.; Tracz, A.; Chwalba, M.; Kozakiewicz, A.; Trzaskowski, B.; Skowerski, K. Cyclic Alkyl Amino Ruthenium Complexes—Efficient Catalysts for Macrocyclization and Acrylonitrile Cross Metathesis. *ACS Catal.* **2017**, *7*, 5443−5449.

(14) (a) Schrodi, Y., Mechanisms of Olefin Metathesis Catalyst Decomposition and Methods of Catalyst Reactivation. In *Handbook of Metathesis*; Grubbs, R. H., Wenzel, A. G., Eds.; Wiley-VCH: Weinheim, 2015; pp 323−342. (b) Chadwick, J. C.; Duchateau, R.; Freixa, Z.; van Leeuwen, P. W. N. M., Alkene Metathesis. *Homogeneous Catalysts: Activity−Stability−Deactivation*; Wiley-VCH: Weinheim, 2011; pp 347−396.

(15) For labile, PPh_3-stabilized [Ru]=CHR catalysts, facile bimolecular coupling can be inferred from many early reports in which stilbenes and related RHC=CHR byproducts were observed. See, for example: (a) Schwab, P.; Grubbs, R. H.; Ziller, J. W. Synthesis and Applications of $RuCl_2(=CHR)(PR_3)_2$. *J. Am. Chem. Soc.* **1996**, *118*, 100−110. (b) Amoroso, D.; Snelgrove, J. L.; Conrad, J. C.; Drouin, S. D.; Yap, G. P. A.; Fogg, D. E. An Attractive Route to Olefin Metathesis Catalysts: Facile Synthesis of a Ruthenium Alkylidene Complex Containing Labile Phosphane Donors. *Adv. Synth. Catal.* **2002**, *344*, 757−763. Observed in (b) were both the olefin byproduct and a structurally characterized ruthenium dimer. For second-generation catalysts, bimolecular coupling was long thought improbable (see ref 14) on the basis of the low concentrations of the 14-electron species arising from strong ligand binding. An additional factor for Grubbs-class catalysts is competing nucleophilic abstraction of the methylidene ligand by PCy_3, even under conditions of catalysis. See: (c) Lummiss, J. A. M.; Ireland, B. J.; Sommers, J. M.; Fogg, D. E. Amine-Mediated Degradation in Olefin Metathesis Reactions that Employ the Second-Generation Grubbs Catalysts. *ChemCatChem* **2014**, *6*, 459−463.

(16) β-Hydride elimination was first explored within d^0 catalysts. For a recent overview, see: (a) Schrock, R. R.; Copéret, C. Formation of High-Oxidation-State Metal−Carbon Double Bonds. *Organometallics* **2017**, *36*, 1884−1892. For leading references to its observation for silica-supported metathesis catalysts, see: (b) Leduc, A.-M.; Salameh, A.; Soulivong, D.; Chabanas, M.; Basset, J.-M.; Copéret, C.; Solans-Monfort, X.; Clot, E.; Eisenstein, O.; Boehm, V. P. W.; Roeper, M.

beta-H Transfer from the metallacyclobutane: a key step in the deactivation and byproduct formation for the well-defined silica-supported rhenium alkylidene alkene metathesis catalyst. *J. Am. Chem. Soc.* **2008**, *130*, 6288−6297. (c) Solans-Monfort, X.; Copéret, C.; Eisenstein, O. Shutting Down Secondary Reaction Pathways: The Essential Role of the Pyrrolyl Ligand in Improving Silica Supported d^0-ML_4 Alkene Metathesis Catalysts from DFT Calculations. *J. Am. Chem. Soc.* **2010**, *132*, 7750−7757.

(17) For labelling studies demonstrating β-hydride elimination from the metallacyclobutane in the Ru systems, see: (a) Romero, P. E.; Piers, W. E. Mechanistic Studies on 14-Electron Ruthenacyclobutanes: Degenerate Exchange with Free Ethylene. *J. Am. Chem. Soc.* **2007**, *129*, 1698−1704. For early experimental and computational evidence, see: (b) Janse van Rensburg, W. J.; Steynberg, P. J.; Meyer, W. H.; Kirk, M. M.; Forman, G. S. DFT Prediction and Experimental Observation of Substrate-Induced Catalyst Decomposition in Ruthenium-Catalyzed Olefin Metathesis. *J. Am. Chem. Soc.* **2004**, *126*, 14332−14333.

(18) For quantitative experimental evidence showing that bimolecular decomposition of $RuCl_2(L)(=CH_2)$ (L = NHC, CAAC) competes with decomposition via β-H elimination, see: (a) Nascimento, D. L.; Fogg, D. E. Origin of the Breakthrough Productivity of Ruthenium-CAAC Catalysts in Olefin Metathesis (CAAC = Cyclic Alkyl Amino Carbene). *J. Am. Chem. Soc.* **2019**, *141*, 19236−19240. (b) Bailey, G. A.; Foscato, M.; Higman, C. S.; Day, C. S.; Jensen, V. R.; Fogg, D. E. Bimolecular Coupling as a Vector for Decomposition of Fast-Initiating Olefin Metathesis Catalysts. *J. Am. Chem. Soc.* **2018**, *140*, 6931−6944. For kinetics evidence of bimolecular decomposition in Ru−NHC systems, see: (c) Thiel, V.; Wannowius, K.-J.; Wolff, C.; Thiele, C. M.; Plenio, H. Ring-Closing Metathesis Reactions: Interpretation of Conversion−Time Data. *Chem. - Eur. J.* **2013**, *19*, 16403−16414.

(19) For reports in which lower metathesis productivity can be seen at higher loadings of the CAAC catalysts, see refs 10−13, 18a, and: (a) Ton, S. J.; Fogg, D. E. The Impact of Oxygen on Leading and Emerging Ru-Carbene Catalysts for Olefin Metathesis: An Unanticipated Correlation Between Robustness and Metathesis Activity. *ACS Catal.* **2019**, *9*, 11329−11334. (b) Blanco, C.; Sims, J.; Nascimento, D. L.; Goudreault, A. Y.; Steinmann, S. N.; Michel, C.; Fogg, D. E. The Impact of Water on Ru-Catalyzed Olefin Metathesis: Potent Deactivating Effects Even at Low Water Concentrations. *ACS Catal.* **2021**, *11*, 893−899.

(20) See ref 18a. Disappearance of the methylidene signal for **1-C1^{Ph}**, $RuCl_2$(**C1^{Ph}**)(py)($=CH_2$), was complete in <5 min at 23 °C in $CDCl_3$, vs just 2% loss of the corresponding **1-H_2IMes**. The latter complex was still observable after 3 h (5% vs internal standard). In both cases, ca. 80% ethylene was ultimately detected (a lower limit, owing to loss of ethylene to the headspace), confirming decomposition via bimolecular coupling.

(21) Foscato, M.; Jensen, V. R. Automated in Silico Design of Homogeneous Catalysts. *ACS Catal.* **2020**, *10*, 2354−2377.

(22) Foscato, M.; Venkatraman, V.; Jensen, V. R. DENOPTIM: Software for Computational de Novo Design of Organic and Inorganic Molecules. *J. Chem. Inf. Model.* **2019**, *59*, 4077−4082.

(23) For a related approach to MCB synthesis that commences with the Hoveyda-class complexes instead, see: Keitz, B. K.; Grubbs, R. H. Probing the Origin of Degenerate Metathesis Selectivity via Characterization and Dynamics of Ruthenacyclobutanes Containing Variable NHCs. *J. Am. Chem. Soc.* **2011**, *133*, 16277−16284.

(24) While the overall trends in k_{rel} remain consistent, the absolute rate constants should be treated with caution: errors ranged from ±5% to 25%, depending on the instability of the species involved. For details, see Figure S1.

(25) Kaczanowska, K.; Trzaskowski, B.; Peszczyńska, A.; Tracz, A.; Gawin, R.; Olszewski, T. K.; Skowerski, K. Cross metathesis with acrylates: N-heterocyclic carbene (NHC)- versus cyclic alkyl amino carbene (CAAC)-based ruthenium catalysts, an unanticipated influence of the carbene type on efficiency and selectivity of the reaction. *ChemCatChem* **2020**, *12*, 6366−6374.

(26) Nascimento, D. L.; Reim, I.; Foscato, M.; Jensen, V. R.; Fogg, D. E. Challenging Metathesis Catalysts with Nucleophiles and Bronsted Base: The Stability of State-of-the-Art Catalysts to Attack by Amines. *ACS Catal.* **2020**, *10*, 11623−11633.

(27) The outstanding performance of **HC2^{Me}** vs **HC1^{Ph}** reported in ethenolysis of methyl oleate (ref 10) is striking in light of the extreme sensitivity of the **C2^{Me}** catalysts to decomposition. Potential contributing factors are the hindered nature of the substrate and the greater steric accessibility of the active species for the **C2^{Me}** catalysts. The drop in TONs from 340 000 to 180 000 on increasing catalyst loadings from 1 ppm to 3 ppm suggests bimolecular decomposition even at very low catalyst concentrations.

(28) Basic aliphatic amines such as $NH_2{}^nBu$ abstract the benzylidene ligand from **GII** or **HII** even at rt. For **GII**, see ref 15c. For **HII**, see: (a) Ireland, B. J.; Dobigny, B. T.; Fogg, D. E. Decomposition of a Phosphine-Free Metathesis Catalyst by Amines and Other Nitrogen Bases: Metallacyclobutane Deprotonation as a Major Deactivation Pathway. *ACS Catal.* **2015**, *5*, 4690−4698. ^{13}C-Labeling studies indicate that *n*-butylamine can compete with PCy_3 to abstract the methylidene ligand from the four-coordinate active species **2-H_2IMes**: (b) Lummiss, J. A. M.; Botti, A. G. G.; Fogg, D. E. Isotopic Probes for Ruthenium-Catalyzed Olefin Metathesis. *Catal. Sci. Technol.* **2014**, *4*, 4210−4218.

(29) Wappel, J.; Urbina-Blanco, C. A.; Abbas, M.; Albering, J. H.; Saf, R.; Nolan, S. P.; Slugovc, C. Halide Exchanged Hoveyda-Type Complexes in Olefin Metathesis. *Beilstein J. Org. Chem.* **2010**, *6*, 1091−1098.

(30) Tracz, A.; Matczak, M.; Urbaniak, K.; Skowerski, K. Nitro-Grela-Type Complexes Containing Iodides − Robust and Selective Catalysts for Olefin Metathesis Under Challenging Conditions. *Beilstein J. Org. Chem.* **2015**, *11*, 1823−1832.

(31) Nechmad, N. B.; Phatake, R.; Ivry, E.; Poater, A.; Lemcoff, N. G. Unprecedented Selectivity of Ruthenium Iodide Benzylidenes in Olefin Metathesis Reactions. *Angew. Chem., Int. Ed.* **2020**, *59*, 3539−3543.

(32) Torker, S.; Khan, R. K. M.; Hoveyda, A. H. The Influence of Anionic Ligands on Stereoisomerism of Ru Carbenes and Their Importance to Efficiency and Selectivity of Catalytic Olefin Metathesis Reactions. *J. Am. Chem. Soc.* **2014**, *136*, 3439−3455.

(33) Blanco, C.; Nascimento, D. L.; Fogg, D. E. Routes to High-Performing Ruthenium-Iodide Catalysts for Olefin Metathesis: Phosphine Lability Is Key to Efficient Halide Exchange. *Organometallics* **2021**, *40*, 1811−1816.

(34) Falivene, L.; Cao, Z.; Petta, A.; Serra, L.; Poater, A.; Oliva, R.; Scarano, V.; Cavallo, L. Towards the online computer-aided design of catalytic pockets. *Nat. Chem.* **2019**, *11*, 872−879.

(35) Gomez-Suarez, A.; Nelson, D. J.; Nolan, S. P. Quantifying and understanding the steric properties of N-heterocyclic carbenes. *Chem. Commun.* **2017**, *53*, 2650−2660.

(36) Paul, U. S. D.; Radius, U. What Wanzlick Did Not Dare To Dream: Cyclic (Alkyl)(amino)carbenes (cAACs) as New Key Players in Transition-Metal Chemistry. *Eur. J. Inorg. Chem.* **2017**, *2017*, 3362−3375.

(37) Paul, U. S. D.; Sieck, C.; Haehnel, M.; Hammond, K.; Marder, T. B.; Radius, U. Cyclic (Alkyl)(Amino)Carbene Complexes of Rhodium and Nickel and Their Steric and Electronic Parameters. *Chem. - Eur. J.* **2016**, *22*, 11005−11014.

(38) Poater, A.; Cosenza, B.; Correa, A.; Giudice, S.; Ragone, F.; Scarano, V.; Cavallo, L. SambVca: A Web Application for the Calculation of the Buried Volume of N-Heterocyclic Carbene Ligands. *Eur. J. Inorg. Chem.* **2009**, *2009*, 1759−1766.

(39) Buried volumes were calculated for the DFT-optimized geometries of **2** using Ru as the center of the sphere, to avoid the skewed orientation of the unsymmetrical CAAC ligands flagged as a concern by Paul and Radius in ref 36.

(40) Hohenstein, E. G.; Sherrill, C. D. Effects of Heteroatoms on Aromatic π−π Interactions: Benzene−Pyridine and Pyridine Dimer. *J. Phys. Chem. A* **2009**, *113*, 878−886.

https://doi.org/10.1021/jacs.1c04424
J. Am. Chem. Soc. 2021, 143, 11072−11079

(41) Nishio, M. The CH/π hydrogen bond in chemistry. Conformation, supramolecules, optical resolution and interactions involving carbohydrates. *Phys. Chem. Chem. Phys.* **2011**, *13*, 13873−13900.
(42) These interactions include donor−acceptor bonding, with the filled π orbitals of the aromatic carbene substituents donating into the π^* and σ^* orbitals of the pyridine N═C and *o*-C−H bonds, respectively (Table S3).
(43) Other donor ligands, such as the isopropoxy group in the leading Grela and Hoveyda catalyst platforms, are also expected to participate in such stabilizing interactions and may indeed contribute to the slow initiation of such CAAC precatalysts. For example, interatomic distances as short as ca. 2.8 Å are seen between the phenyl ring of the **C1**$^{\mathbf{Ph}}$ ligand and the chelated isopropoxy donor in the X-ray crystal structure of **nG-C1**$^{\mathbf{Ph}}$ (ref 13).
(44) Fernández-Ramos, A.; Miller, J. A.; Klippenstein, S. J.; Truhlar, D. G. Modeling the Kinetics of Bimolecular Reactions. *Chem. Rev.* **2006**, *106*, 4518−4584.
(45) Álvarez-Moreno, M.; de Graaf, C.; López, N.; Maseras, F.; Poblet, J. M.; Bo, C. Managing the Computational Chemistry Big Data Problem: The ioChem-BD Platform. *J. Chem. Inf. Model.* **2015**, *55*, 95−103.

https://doi.org/10.1021/jacs.1c04424
J. Am. Chem. Soc. 2021, 143, 11072−11079